Parallel and perpendicular transport in multilayered structures

Y. Asano, A. Oguri, and S. Maekawa
Department of Applied Physics, Nagoya University, Nagoya 464-01, Japan
(Received 2 February 1993; revised manuscript received 26 April 1993)

The difference between parallel and perpendicular conductance in magnetic superlattices such as Fe/Cr are studied numerically with the Kubo formula and a recursion method. In the calculation, the multilayered structure of superlattices is taken into account through a periodic potential along the direction normal to the interfaces. It is shown that the magnetoresistance for the current parallel to the layers $MR_{\parallel}$ is increased by the interface roughness and decreased by the bulk impurity scattering. Since the Brillouin zone is divided into a series of minizones due to the periodic potential, the magnetoresistance for the current perpendicular to the layers $MR_{\perp}$ is determined by the miniband structure and becomes larger than $MR_{\parallel}$.

I. INTRODUCTION

The giant magnetoresistance (MR) observed in magnetic superlattices, such as Fe/Cr, has stimulated a great deal of investigation of transport phenomena in metallic superlattices.[1-7] In Fe/Cr superlattices, the magnetization in adjacent Fe layers is aligned antiferromagnetically in the absence of an external magnetic field. The magnetization changes to the ferromagnetic alignment by an applied field, and the electric resistance with the current parallel to the layers decreases by 45%.[1] In recent experiments, giant MR was observed also with the current applied perpendicular to the layers in Co/Ag superlattices.[8]

Intensive theoretical studies of the giant MR have been done.[9-21] It was pointed out that the interface roughness plays an important role in the giant MR. However, our understanding of the influence of the multilayered structure on the transport properties is still at an early stage. In a previous work[20] we proposed a tight-binding model for a superlattice, in which the multilayered structure is treated as a periodic potential along the direction normal to the interfaces. Based on this model, we have calculated the conductance for the current parallel to the layers $\Gamma_{\parallel}$ in two-dimensional superlattices using the Landauer formalism with the transfer matrix method.[20] Although the system size is limited, no further approximation is needed for our numerical method. Independently, Bauer has applied the Landauer formalism to magnetic superlattices and examined the conductance for the current perpendicular to the layers $\Gamma_{\perp}$ within the Born approximation.[21]

The purpose of this paper is to study the difference between the parallel and the perpendicular conductances. To this end, we calculate the conductance in two- (2D) and three- (3D) dimensional superlattices numerically within the Kubo formalism using the recursion method.[22] It was proved rigorously that the Landauer formalism is derived from the Kubo formula for a finite system with perfect lead wires.[23] Thus, the definition of the conductance used in this paper is exactly the same as the one used in a previous work.[20] We use the Kubo formalism because it is convenient for numerical calculation for large systems. In order to clarify effects purely due to the multilayered structure, we examine the conductance in nonmagnetic superlattices. We find that $\Gamma_{\parallel}$ is larger than $\Gamma_{\perp}$ both in 2D and 3D. This is due to the fact that the Brillouin zone is divided into a series of minizones in the direction perpendicular to the layers. Then we apply the recursion method to Fe/Cr magnetic superlattices. We find that the magnetoresistance for the current parallel to the layers $MR_{\parallel}$ is increased by the interface roughness and decreased by the bulk impurity scattering. The current perpendicular to the layers is strongly affected by the structure of the minibands, and the magnetoresistance in this direction, $MR_{\perp}$, becomes larger than $MR_{\parallel}$.

The outline of the paper is as follows. In Sec. II, the model is introduced, and the numerical method is briefly explained. In Sec. III, the parallel and perpendicular conductances in nonmagnetic superlattices is presented. In Sec. IV, the magnetoresistance in Fe/Cr magnetic superlattices is studied. Conclusions are given in Sec. V.

II. METHOD

Let us consider the tight-binding model on the lattices in which one of the dimensions (the x direction) is much larger than the others, i.e., a long-strip lattice in 2D and a long-bar lattice in 3D. The Hamiltonian is given by

$$H=-t\sum_{\langle i\mathbf{n},j\mathbf{m}\rangle,\sigma}c^{\dagger}_{i,\mathbf{n},\sigma}c_{j,\mathbf{m},\sigma}+\sum_{i,\mathbf{n},\sigma}\varepsilon_{i,\mathbf{n}}c^{\dagger}_{i,\mathbf{n},\sigma}c_{i,\mathbf{n},\sigma}-\sum_{i,\mathbf{n},\alpha,\beta}\mathcal{M}_{i,\mathbf{n}}c^{\dagger}_{i,\mathbf{n},\alpha}\sigma_{\alpha,\beta}c_{i,\mathbf{n},\beta}\,, \tag{1}$$

where i and j label the sites in the x direction, $\mathbf{n}$ and $\mathbf{m}$ are the vectors in the transverse directions, $c^{\dagger}_{i,\mathbf{n},\alpha}$ is the creation operator of an electron with spin α at site $(i,\mathbf{n})$, $\varepsilon_{i,\mathbf{n}}$ is the on-site potential, $\mathcal{M}_{i,\mathbf{n}}$ is the exchange potential in the magnetic ion, and σ's are the Pauli matrices. The summation $\langle i\mathbf{n},j\mathbf{m}\rangle$ runs over nearest-neighbor sites. In what follows energy is measured in units of the transfer integral t and length is measured in units of the lattice constant.

The system consists of three regions as shown in Fig. 1: a sample of length L $(1\le i\le L)$, and two perfect lead

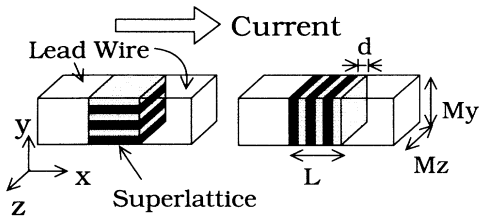

(a) Parallel (b) Perpendicular

FIG. 1. Configurations of the system for the current (a) parallel and (b) perpendicular to the layers. Here d denotes the thickness of each layer, L is the length of the superlattice in the x direction, and M_y and M_z are the width in the y and z directions, respectively.

wires attached to both sides of the sample, i.e., $(-\infty \le i \le 0)$ and $(L+1 \le i \le \infty)$. In the transverse direction, the widths M_y and M_z are finite, and a free boundary condition is used. Thus, electronic states in the lead wire consists of a number of subbands. The multilayered structure of a superlattice is taken into account through the $(i,\mathbf{n})$ dependence of $\varepsilon_{i,\mathbf{n}}$ and $\mathcal{M}_{i,\mathbf{n}}$ in the region $1 \le i \le L$. For example, in a nonmagnetic A/B superlattice, the on-site and the exchange potentials are given by

$$\mathcal{M}_{i,\mathbf{n}}=0 ,$$
$$\varepsilon_{i,\mathbf{n}}=\begin{cases}\varepsilon_A: & (i,\mathbf{n})\in A \text{ layer} ,\\ \varepsilon_B: & (i,\mathbf{n})\in B \text{ layer} .\end{cases} \tag{2}$$

Here, ε_A and ε_B are the on-site potentials in the A and B atoms, respectively. In the lead wires the potential are constant, i.e., $\varepsilon_{i,\mathbf{n}}=0$ and $\mathcal{M}_{i,\mathbf{n}}=0$. When the level spacing of the subbands is much smaller than the Fermi energy E_F, the number of the subbands at E_F becomes large. In such a case, this model may be good for a metal. Thus, in general, it is desirable to use a sufficiently large system. In our calculation the number of the subbands at E_F is about 100 in the lead wire, so that we believe our results are applicable to a metal.

The Green's function is defined by

$$G^{\pm}(i,j)_{\mathbf{n}\sigma,\mathbf{m}\sigma'}\equiv\left\langle i,\mathbf{n},\sigma\left|\frac{1}{E-H\pm i\eta}\right|j,\mathbf{m},\sigma'\right\rangle ,$$
$$|i,\mathbf{n},\sigma\rangle\equiv c^{\dagger}_{i,\mathbf{n},\sigma}|0\rangle , \tag{3}$$

where $|0\rangle$ denotes vacuum, $i\eta$ is an infinitesimally small imaginary part. We introduce another Green's function[22]

$$G^{L\pm}(i_0)_{\mathbf{n}\sigma,\mathbf{m}\sigma'}\equiv\left\langle i_0,\mathbf{n},\sigma\left|\frac{1}{E-H^{(i_0)}\pm i\eta}\right|i_0,\mathbf{m},\sigma'\right\rangle , \tag{4}$$

where $H^{(i_0)}$ is the Hamiltonian for a system in which all sites $i > i_0$ are deleted. In what follows, we treat $G^{L\pm}(i_0)$ as a 2×2 matrix for 1D, and as $2M_y\times 2M_y$ and $2M_yM_z\times 2M_yM_z$ matrices for 2D and 3D, respectively. In a D-dimensional system $G^{L\pm}(i_0)$ obeys the matrix recursion relation

$$G^{L}(i_0)=[G^{0}(i_0)^{-1}-t^2G^{L}(i_0-1)]^{-1} , \tag{5}$$

where $G^0(i_0)$ is the Green's function for the isolated $(D-1)$-dimensional sheet at $x=i_0$. It is shown that

$$G(i,i)=[G^0(i)^{-1}-t^2G^R(i+1)-t^2G^L(i-1)]^{-1} \tag{6}$$

and

$$G(i,i+1)=-tG(i,i)G^R(i+1) . \tag{7}$$

Here $G^R(i_0)$ is the Green's function for a system in which all sites $i < i_0$ are deleted. Initially $G^L(i)$ is computed for the left perfect lead wire $(-\infty \le i \le 0)$. Then $G^L(i)$ for the left lead wire plus the sample $(-\infty \le i \le L)$ is obtained by use of Eq. (5). Finally another perfect lead wire $(L+1 \le i \le \infty)$ is attached to the sample, and $G^{\pm}(i,j)$ is calculated from Eqs. (6) and (7).

The conductance Γ is given by the Kubo formula

$$\Gamma=\frac{4e^2t^2}{h}\mathrm{Tr}[\tilde{G}(i,i)\tilde{G}(i-1,i-1)+\tilde{G}(i-1,i-1)\tilde{G}(i,i)-\tilde{G}(i,i-1)\tilde{G}(i,i-1)-\tilde{G}(i-1,i)\tilde{G}(i-1,i)] , \tag{8}$$

with

$$\tilde{G}(i,i')\equiv\frac{1}{2i}\{G^{-}(i,i')-G^{+}(i,i')\} ,$$

where i and i' are arbitrary. In this method, the upper bound of the conductance is given by

$$\Gamma_{\max}\equiv\frac{2e^2}{h}M_yM_z , \tag{9}$$

which is for the sample with no imperfection, i.e., $\varepsilon_{i,\mathbf{n}}\equiv 0$ and $\mathcal{M}_{i,\mathbf{n}}\equiv 0$. The density of states per spin is also calculated from $\tilde{G}(i,i)$:

$$\rho(E)=\frac{1}{2\pi LM_yM_z}\sum_{i\in\text{sample}}\mathrm{Tr}[\tilde{G}(i,i)] . \tag{10}$$

III. CONDUCTANCE IN NONMAGNETIC SUPERLATTICES

Before discussing the giant magnetoresistance in Fe/Cr, the effects due purely to the multilayered structure should be clarified. In this section, the conductance in a nonmagnetic A/B superlattice is studied. We use the parameter ε_S for the periodic on-site potential, $\varepsilon_A=-\varepsilon_B(=\varepsilon_S)$, and measure the conductance in units of $2e^2/h$.

The results for a 1D superlattice are shown as a function of the Fermi energy E_F in Fig. 2, where $\varepsilon_S=1.0$, $L=48$, and the thickness of each layer is $d=4$. In the calculation the infinitesimally small imaginary part for the Green's function η is taken to be $\eta\to 0$ for the conductance, and $\eta=0.01$ for the density of states (per site). The density of states is separated into $2d$ minibands because the on-site potential is periodic, and four of them are seen in Fig. 2. Since electrons are reflected at the boundaries between the sample and the lead wires, at $x=0$ and L, the conductance becomes smaller than $\Gamma_{\max}(=1)$. The oscillation of the conductance is due to

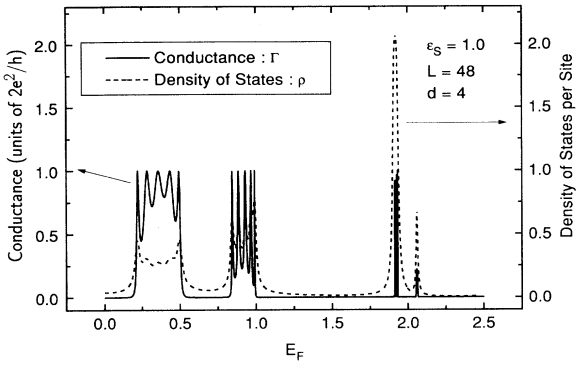

FIG. 2. The conductance and the density of states per site in a 1D superlattice. Here only the results for $E_F \geq 0$ are shown since the results for $E_F \leq 0$ are symmetric about the band center $E_F = 0$. Energy is measured in units of t.

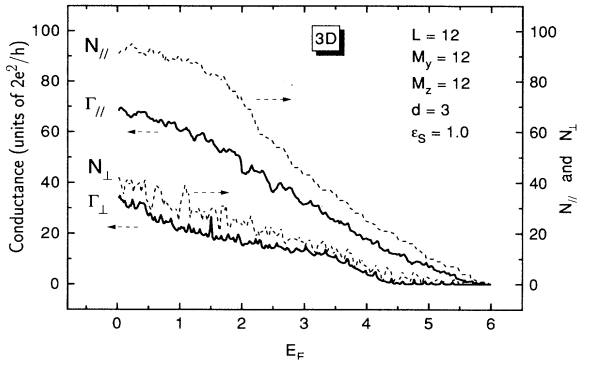

FIG. 4. E_F dependence of the conductance Γ and the number of subbands N for the parallel ($\|$) and the perpendicular ($\perp$) configurations. Energy is measured in units of t.

interference effects. Typically, the conductance is of the order of 1.0 when E_F is in a miniband, while it is almost zero when E_F is in an energy gap.

The conductance depends on the direction of the current in higher dimensions. In Fig. 1, the configurations of the system for the parallel and perpendicular conductances are shown. Since electrons are confined in a finite region along the y and z directions, the wave function for these directions is given by a set of normal modes, i.e., subbands, with discrete eigenvalues. The structure of the subbands in the two configurations are shown schematically in Fig. 3, where k_x is the wave number in the x direction. In the parallel configuration the on-site potential is periodic along the y direction, so that the eigenvalues are changed by the periodicity. On the other hand, in the perpendicular configuration the eigenvalues are not changed, but each subband is divided into a series of minibands due to the periodicity along the x direction. In Fig. 4, E_F dependence of the conductance is shown, where $\varepsilon_S = 1.0$, $L = 12$, $M_y = 12$, $M_z = 12$, and $d = 3$. Thus, the system used in the calculation consists of four blocks, $A/B/A/B$, and each block contains three monolayers. The conductance for the parallel configuration $\Gamma_\|$ is larger than that for the perpendicular configuration $\Gamma_\perp$. In Fig. 5, $\Gamma_\|$ and $\Gamma_\perp$ in a 2D superlattice are shown, where $L = 48$, $M_y = 48$, and $d = 4$. The same feature is also seen in 2D. We note that the wavelength is of the order of the lattice constant when E_F is around the center of the conduction band, and is much larger than the lattice constant when E_F is near the band edge. In Figs. 4 and 5, the number of subbands which have finite density of states at E_F are also shown, where $N_\|$ ($N_\perp$) is the number of such subbands for the parallel (perpendicular) configuration. The E_F dependence of $N_\|$ ($N_\perp$) is similar to $\Gamma_\|$ ($\Gamma_\perp$). Since only the states at E_F carry the current, the conductance is determined mainly by the number of subbands with finite density of states. If we consider the thermodynamic limit, the energy $E_{k_\|,k_\perp}$ is continuous as a function of $k_\|$ and has discontinuities as a function of $k_\perp$, where $k_\|$ and $k_\perp$ are parallel and perpendicular components of the wave vector, respectively. Thus, it is expected that the discontinuities or the structure of the minibands will determine the perpendicular transport also in an infinitely large system.

So far, we have discussed a superlattice with no disorder. In actual superlattices, the A and B atoms are distributed randomly near the interfaces. We introduce the parameter λ to characterize the interface roughness. In an A layer, each A atom next to a B layer is replaced by a B atom with a probability λ. Similarly, in a B layer, each B atom next to an A layer is replaced by an A atom with the same probability λ. A typical example of a sam-

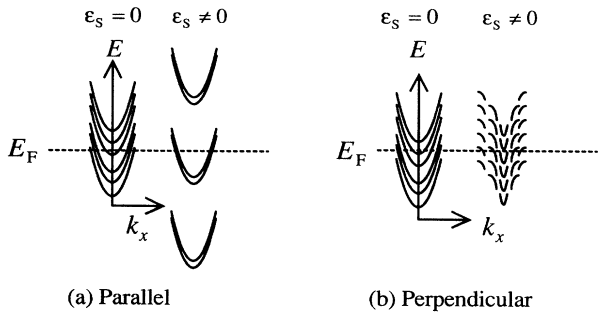

FIG. 3. Schematic figures of the structure of the subbands for (a) parallel, and (b) perpendicular configurations.

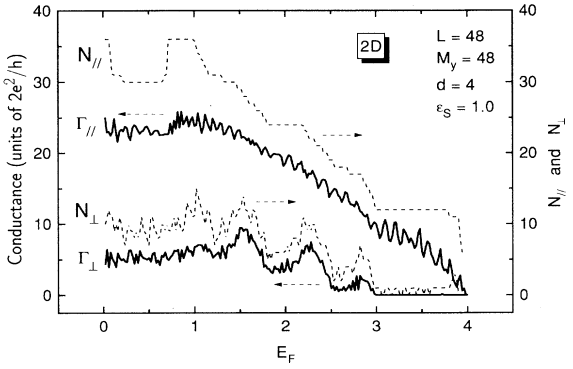

FIG. 5. The conductance and the number of subbands in a 2D nonmagnetic superlattice. Energy is measured in units of t.

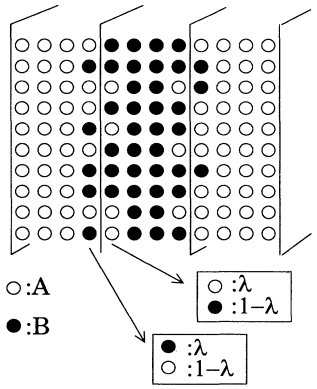

FIG. 6. A schematic figure of a sample with rough interfaces. The open and solid circles denote A and B atoms, respectively.

ple with rough interfaces is shown in Fig. 6. The λ dependence of $\Gamma_{\parallel}$ and $\Gamma_{\perp}$ is shown in Fig. 7 with several choices of E_F. The results are obtained by averaging over 100 different samples, and the error bars are smaller than the size of the symbols. Since the parameter λ corresponds to the concentration of the impurities, the conductance decrease is proportional to λ near $\lambda \approx 0$, as is given by the Born approximation. However, when λ increases above $\lambda \approx 0.05$, the conductance deviates from the linear relation. The difference between $\Gamma_{\parallel}$ and $\Gamma_{\perp}$ decreases with increasing interface roughness. We next examine the effect of bulk impurity scattering by introducing the parameter W_B. The on-site potential in each A and B atom is changed randomly in the range

$$\begin{aligned} &\varepsilon_S - \frac{W_B}{2} \le \varepsilon_A \le \varepsilon_S + \frac{W_B}{2} , \\ &-\varepsilon_S - \frac{W_B}{2} \le \varepsilon_B \le -\varepsilon_S + \frac{W_B}{2} . \end{aligned} \tag{11}$$

The W_B dependence of the conductance is shown with several choices of E_F in Fig. 8. The conductance decreases proportionally to W_B^2 for small W_B. For large

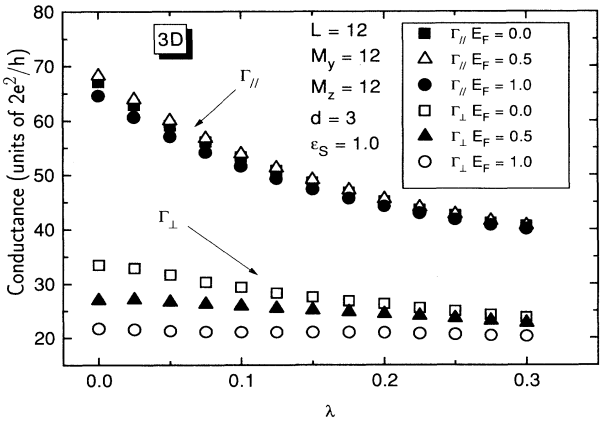

FIG. 7. $\Gamma_{\parallel}$ and $\Gamma_{\perp}$ as functions of the interface roughness λ, where $E_F = 0.0$, 0.5, and 1.0. The results are obtained by averaging over 100 different samples.

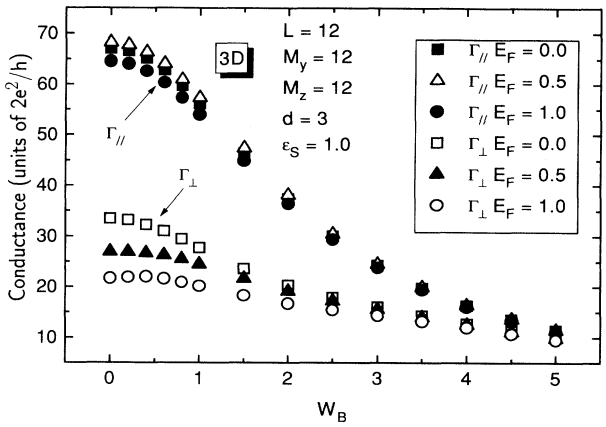

FIG. 8. $\Gamma_{\parallel}$ and $\Gamma_{\perp}$ as functions of the bulk impurity scattering W_B.

W_B, the conductance does not depend on the direction of the current because the effects of the multilayered structure are destroyed by the bulk impurities.

IV. MAGNETORESISTANCE IN Fe/Cr SUPERLATTICES

In Fe/Cr superlattices, the magnetization in adjacent Fe layers is aligned antiferromagnetically (AF) in the absence of an external magnetic field. The magnetization is changed to the ferromagnetic (F) alignment by an applied field. Thus, the difference between the resistance in the two alignments corresponds to the magnetoresistance, which is defined by

$$\mathrm{MR} \equiv \frac{R(\mathrm{AF}) - R(\mathrm{F})}{R(\mathrm{AF})} , \tag{12}$$

where R(AF) and R(F) are the electrical resistances in the AF and F alignments, respectively. There is a relation among the potentials in the Fe/Cr superlattice:[14]

$$\varepsilon_{\mathrm{Fe}} + |\mathcal{M}| \approx \varepsilon_{\mathrm{Cr}} , \tag{13}$$

where $\varepsilon_{\mathrm{Fe}}$ ($\varepsilon_{\mathrm{Cr}}$) is the on-site potential for an Fe (Cr) atom, and $\mathcal{M}$ is the exchange potential for an Fe atom. The exchange potential is zero for a nonmagnetic Cr ion. In Eq. (13), $\varepsilon_{\mathrm{Fe}} + |\mathcal{M}|$ is the potential energy for an electron whose spin direction is opposite to $\mathcal{M}$ ($\downarrow$ electron). Thus, in the F alignment the potential for the $\downarrow$ electron in the Fe layer is almost the same as that in the Cr layer as illustrated in Fig. 9, so that the $\downarrow$ electrons are scattered only weakly when Fe and Cr atoms are distributed randomly at the interfaces.

In the following, we examine the parallel and perpendicular transport in Fe/Cr using a finite system with $L = 12$, $M_y = 12$, $M_z = 12$, and $d = 3$. This system consists of four blocks, Fe/Cr/Fe/Cr, as shown in Fig. 9, and electrons feel a different potential depending on the spin σ and the alignment of magnetization of Fe layers as illustrated in this figure. In Fig. 10, the parallel conductance for the electrons with spin σ in the AF and F alignments, $\Gamma_{\parallel}^{\mathrm{AF}\sigma}$ and $\Gamma_{\parallel}^{\mathrm{F}\sigma}$, are shown as a function of the in-

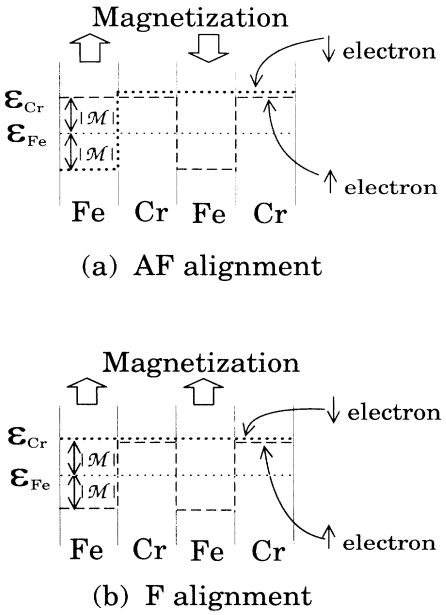

FIG. 9. Schematic figures of the potential in Fe/Cr superlattices for the electrons with spin ↑ and ↓ in the (a) AF and (b) F alignments. Here ε_{Cr} (ε_{Fe}) is the on-site potential for a Cr (Fe) atom, and $\mathcal{M}$ is the exchange potential for an Fe atom.

terface roughness, where the Fermi energy is fixed at $E_F=0.0$ and the conductance is measured in units of e^2/h. The potentials are taken to be $\varepsilon_{Cr}=0.5$, $\varepsilon_{Fe}=-0.5$, and $|\mathcal{M}|=1.0$ so as to satisfy the relation $\varepsilon_{Fe}+|\mathcal{M}|=\varepsilon_{Cr}$. Thus, $\Gamma_{\parallel}^{F\downarrow}$ is a constant independent of λ. The other conductances $\Gamma_{\parallel}^{F\uparrow}$, $\Gamma_{\parallel}^{AF\uparrow}$, and $\Gamma_{\parallel}^{AF\downarrow}$ decrease with increasing λ due to the scattering by the interface roughness. Because of the limitation of sample size and/or the existence of the boundary in the y-z plane, the conductance in the AF alignment depends on the spin σ. The magnetoresistance for the parallel configuration $MR_{\parallel}$ is obtained by using Eq. (12) and the electrical resistance

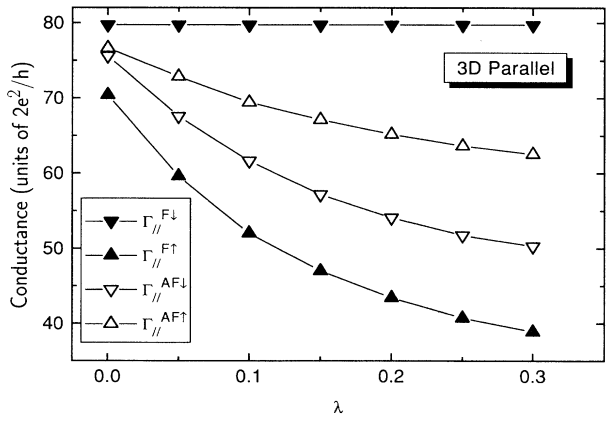

FIG. 10. The parallel conductance for the electrons with spin σ in the AF and F alignments ($\Gamma_{\parallel}^{AF\sigma}$ and $\Gamma_{\parallel}^{F\sigma}$) as a function of λ. The results are obtained by averaging over 100 different samples.

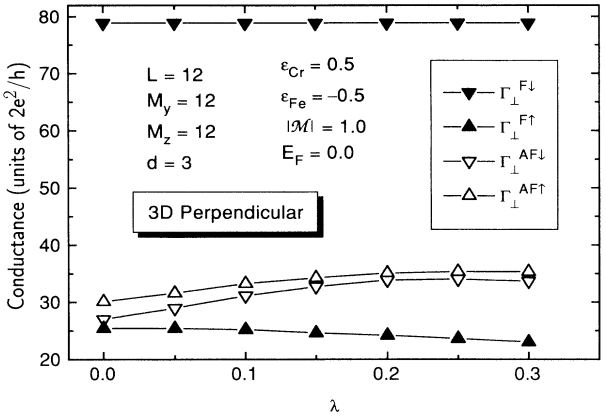

FIG. 11. The perpendicular conductances for the electrons with spin σ in the AF and F alignments ($\Gamma_{\perp}^{AF\sigma}$ and $\Gamma_{\perp}^{F\sigma}$) as functions of λ.

$$R=(\Gamma^{\uparrow}+\Gamma^{\downarrow})^{-1} . \tag{14}$$

Since the difference between $R_{\parallel}$(F) and $R_{\parallel}$(AF) increases with the interface roughness, $MR_{\parallel}$ increases with λ as shown in Fig. 12. This tendency is seen to be more pronounced in a 2D system, which is shown in Fig. 13, where $L=48$, $M_y=48$, and $d=4$. The λ dependence of $MR_{\parallel}$ indicates that the interface roughness plays an important role in the giant magnetoresistance.

The perpendicular conductance for the electrons with spin σ in the AF and F alignments, $\Gamma_{\perp}^{AF\sigma}$ and $\Gamma_{\perp}^{F\sigma}$, are shown in Fig. 11, where the potentials and other parameters are the same as those used in Fig. 10. In the F alignment, the conductance for the ↓ electrons does not depend on the configuration $\Gamma_{\perp}^{F\downarrow}=\Gamma_{\parallel}^{F\downarrow}$ because of the relation $\varepsilon_{Fe}+|\mathcal{M}|=\varepsilon_{Cr}$. The other conductances $\Gamma_{\perp}^{F\uparrow}$, $\Gamma_{\perp}^{AF\downarrow}$, and $\Gamma_{\perp}^{AF\uparrow}$ are much smaller than $\Gamma_{\perp}^{F\downarrow}$, which is determined by the structure of the minibands due to the periodic potential. In Fig. 12, the magnetoresistance for the perpendicular configuration $MR_{\perp}$ is shown. Since $R_{\perp}$(AF) is larger than $R_{\perp}$(F), $MR_{\perp}$ is finite even at $\lambda=0$ where the electrical resistance is caused by the contact potential between the sample and the lead wires. For

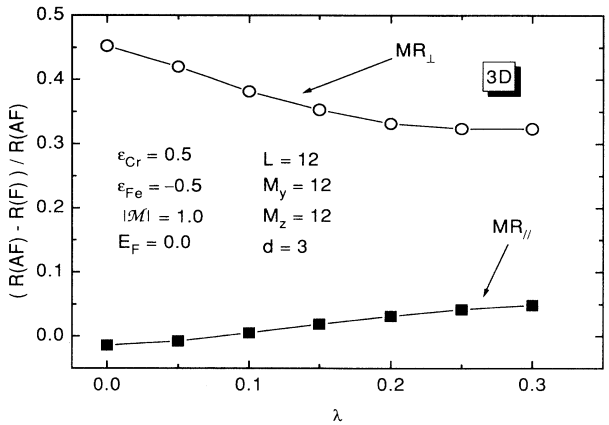

FIG. 12. The magnetoresistance in Fe/Cr as a function of the interface roughness λ.

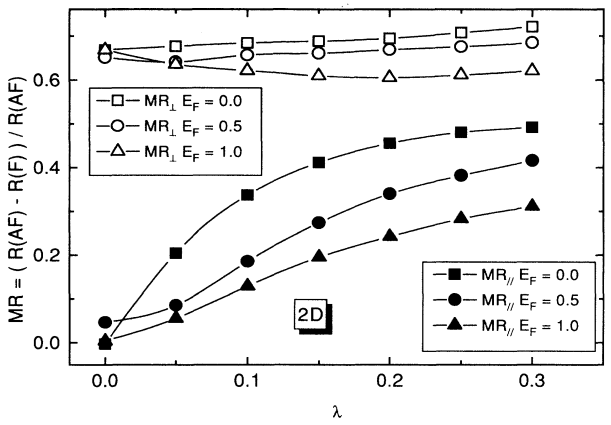

FIG. 13. The parallel and perpendicular magnetoresistance in 2D Fe/Cr.

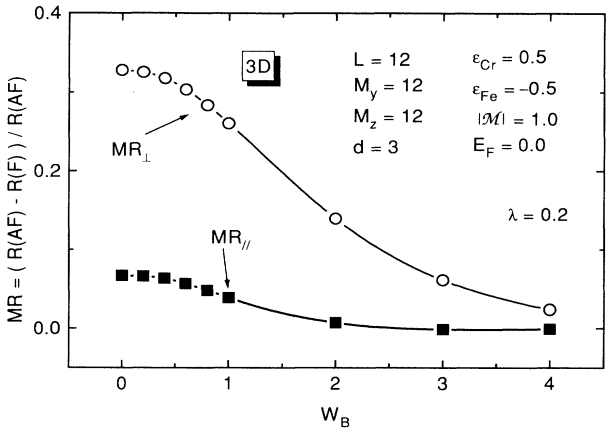

FIG. 14. The MR of Fe/Cr as a function in bulk impurity scattering W_B, where λ is fixed at 0.2.

small λ, $\Gamma_{\perp}^{AF\uparrow}$ and $\Gamma_{\perp}^{AF\downarrow}$ increase with λ (or the interface roughness), so that $MR_{\perp}$ decreases with increasing λ. This is caused by the fact that the impurity levels are created in the gap between the minibands and contribute to the current. Whether $MR_{\perp}$ increases or not is determined by E_F as shown in Fig. 13, where $MR_{\perp}$ in the 2D system is given with several choices of E_F. The perpendicular magnetoresistance is sensitive to the structure of minibands.

We next examine effects of the bulk impurity scattering. In Fig. 14, the magnetoresistance is shown as a function of the parameter W_B define in Eq. (11). Here the interface roughness λ is fixed at 0.2. The magnetoresistances $MR_{\parallel}$ and $MR_{\perp}$ decrease with increasing W_B. This is because the relation Eq. (13) does not hold at impurity sites and the ↓ electrons in the F alignment are also scattered. Therefore, the magnetoresistance in Fe/Cr superlattices is suppressed by the bulk impurity scattering. It has been observed experimentally that $MR_{\parallel}$ in Fe/Cr increases with increasing the interface roughness consistent with theoretical results.[6] Experiments to examine the effects of the bulk impurity scattering on $MR_{\parallel}$ are expected.

Our results show that $MR_{\perp}$ is larger than $MR_{\parallel}$. Experimentally the magnetoresistance for both configurations has been observed in Co/Ag superlattices, and it was confirmed that $MR_{\perp} > MR_{\parallel}$.[8] Since the electronic structure in Ag is different from that in transition metals, the argument in this section does not apply immediately to Co/Ag. Experiments in Fe/Cr are desirable.

V. CONCLUSIONS

In this paper, the parallel and perpendicular transport in multilayered structure was studied based on a tight-binding model with a periodic potential along one of the dimensions. The perpendicular transport is determined mainly by the structure of the minibands (or the gap) caused by the periodic potential. On the other hand, the parallel transport is not affected as much by the miniband structure, and the parallel conductance $\Gamma_{\parallel}$ is larger than the perpendicular conductance $\Gamma_{\perp}$.

The giant magnetoresistance in magnetic Fe/Cr superlattices was examined in light of the present theory. The parallel magnetoresistance $MR_{\parallel}$ is increased by interfaces roughness, and is suppressed by bulk impurity scattering. The miniband structure of the superlattices plays an important role in the perpendicular transport, and the magnetoresistance $MR_{\perp}$ becomes larger than $MR_{\parallel}$. The recursion method may also be applied to various periodic systems such as a CoCu granular alloy.[24,25] Results for the granular alloys will be given elsewhere.

Recently the authors became aware that the magnetoresistance for both parallel $MR_{\parallel}$ and perpendicular configuration $MR_{\perp}$ in Fe/Cr has been measured by M. A. M. Gijs *et al.*[26] In the measurement, it was observed that $MR_{\perp}$ is larger than $MR_{\parallel}$ at low temperatures.

ACKNOWLEDGMENTS

We would like to thank J. Inoue and H. Itoh for various discussions. This work was supported by a Grant-in-Aid for Scientific Research on Priority Areas from the Ministry of Education, Science and Culture.

[1]M. N. Baibich, J. M. Broto, A. Fert, F. Nguyen Van Dau, F. Petroff, P. Etienne, G. Creuzet, A. Friederich, and J. Chazelas, Phys. Rev. Lett. **61**, 2472 (1988).

[2]T. Shinjo and H. Yamamoto, J. Phys. Soc. Jpn. **59**, 2472 (1990).

[3]D. H. Mosca, F. Petroff, A. Fert, P. A. Schroeder, W. P. Pratt, Jr., and R. Laloee, J. Magn. Magn. Mater. **94**, L1 (1991).

[4]S. S. P. Parkin, R. Bhadra, and K. P. Roche, Phys. Rev. Lett. **66**, 2152 (1991).

[5]P. Grünberg, R. Schreiber, Y. Pang, M. B. Brodsky, and H. Sowers, Phys. Rev. Lett. **57**, 2442 (1986).

[6]E. E. Fullerton, D. M. Kelly, J. Guimpel, and I. K. Schuller, Phys. Rev. Lett. **68**, 859 (1992).

[7]K. Takanashi, Y. Obi, Y. Mitani, and H. Fujimori, J. Phys. Soc. Jpn. **61**, 1169 (1992).
[8]W. P. Pratt, Jr., S.-F. Lee, J. M. Slaughter, R. Loloee, P. A. Schroeder, and J. Bass, Phys. Rev. Lett. **66**, 3060 (1991).
[9]R. E. Camley and J. Barnas, Phys. Rev. Lett. **63**, 664 (1989).
[10]P. M. Levy, S. Zhang, and A. Fert, Phys. Rev. Lett. **65**, 1463 (1990).
[11]S. Zhang and P. M. Levy, J. Appl. Phys. **69**, 4786 (1991).
[12]S. Zhang, P. M. Levy, and A. Fert, Phys. Rev. B **45**, 8689 (1992).
[13]M. Johnson, Phys. Rev. Lett. **67**, 3594 (1991).
[14]J. Inoue, A. Oguri, and S. Maekawa, J. Phys. Soc. Jpn. **60**, 376 (1991).
[15]J. Inoue and S. Maekawa, Prog. Theor. Phys. Suppl. **106**, 187 (1991).
[16]J. Inoue, H. Itoh, and S. Maekawa, J. Phys. Soc. Jpn. **61**, 1149 (1992).
[17]H. Itoh, J. Inoue, and S. Maekawa, Phys. Rev. B **47**, 5809 (1993).
[18]A. Okiji, H. Nakanishi, K. Sakata, and H. Kasai, Jpn. J. Appl. Phys. **31**, L806 (1992).
[19]H. Hasegawa, Phys. Rev. B **47**, 15 073 (1993); **47**, 15 080 (1993).
[20]A. Oguri, Y. Asano, and S. Maekawa, J. Phys. Soc. Jpn. **61**, 2652 (1992).
[21]G. E. W. Bauer, Phys. Rev. Lett. **69**, 1676 (1992).
[22]P. A. Lee and D. S. Fisher, Phys. Rev. Lett. **47**, 882 (1981).
[23]D. S. Fisher and P. A. Lee, Phys. Rev. B **23**, 6851 (1981).
[24]A. E. Berkowitz, J. R. Mitchell, M. J. Carey, A. P. Young, S. Zhang, F. E. Spada, F. T. Parker, A. Hutten, and G. Thomas, Phys. Rev. Lett. **68**, 3745 (1992).
[25]J. Q. Xiao, J. S. Jiang, and C. L. Chien, Phys. Rev. Lett. **68**, 3749 (1992).
[26]M. A. M. Gijs, S. K. J. Lenczowski, and J. B. Giesbers, Phys. Rev. Lett. **70**, 3343 (1993).